OPEN ACCESS
Journal of Innovative Optical Health Sciences
Vol. 16, No. 4 (2023) 2250033 (9 pages)

DOI: 10.1142/S179354582250033X

World Scientific
www.worldscientific.com

Lipid droplets imaging with three-photon microscopy

Mubin He[*,††], Hojeong Park[†,††], Guangle Niu[‡], Qiming Xia[§], Hequn Zhang[*], Ben Zhong Tang[¶,‖] and Jun Qian[*,**]

[*]*State Key Laboratory of Modern Optical Instrumentations*
Centre for Optical and Electromagnetic Research
College of Optical Science and Engineering
International Research Center for Advanced Photonics
Zhejiang University, Hangzhou 310058, P. R. China

[†]*Department of Chemistry, The Hong Kong Branch of Chinese*
National Engineering Research Center for Tissue Restoration and Reconstruction
The Hong Kong University of Science and Technology
Clear Water Bay, Kowloon, Hong Kong 999077, P. R. China

[‡]*Shenzhen Research Institute of Shandong University*
Shenzhen 518057, P. R. China

[§]*Department of General Surgery, Sir Run Run Shaw Hospital*
School of Medicine, Zhejiang University
Hangzhou 310000, P. R. China

[¶]*School of Science and Engineering*
Shenzhen Institute of Aggregate Science and Technology
The Chinese University of Hong Kong
Shenzhen, Guangdong 518172, P. R. China
[‖]*tangbenz@cuhk.edu.cn*
[**]*qianjun@zju.edu.cn*

Received 21 May 2022
Accepted 1 August 2022
Published 14 October 2022

Lipid droplets (LDs) participate in many physiological processes, the abnormality of which will cause chronic diseases and pathologies such as diabetes and obesity. It is crucial to monitor the distribution of LDs at high spatial resolution and large depth. Herein, we carried three-photon imaging of LDs in fat liver. Owing to the large three-photon absorption cross-section of the luminogen named NAP-CF_3 (1.67×10^{-79} cm^6 s^2), three-photon fluorescence fat liver imaging

[‖,**]Corresponding authors.
[††]Mubin He and Hojeong Park contributed equally to this paper.

reached the largest depth of 80 μm. Fat liver diagnosis was successfully carried out with excellent performance, providing great potential for LDs-associated pathologies research.

Keywords: Lipid droplets; three-photon fluorescence microscopy; fat liver, deep-tissue imaging.

1. Introduction

Lipid droplets (LDs) are intracellular organelles for storing neutral lipids, including triglycerides and cholesterol esters, which are widely present in adipocytes, hepatocytes, and the adrenal cortex.[1] LDs are involved in many physiological processes, including membrane synthesis and trafficking,[2] inflammation,[3] and protein degradation,[4] and are associated with chronic diseases pathologies such as diabetes, obesity, atherosclerosis, and viral replication.[5] Thus, it is critically important to image LDs for localization and analysis in biomedical research and clinical diagnosis.

Optical imaging is preferred for the location and analysis of LDs due to its high spatial resolution, real-time performance, and specifically staining ability. Many optical imaging technologies have been applied to LDs imaging, including confocal laser scanning microscopy (CLSM),[6–9] Raman microscopy,[10] and multi-photon microscopy.[11–17] CLSM enables high spatial-resolution performance of LD imaging, while super-resolution microscopy including stimulated emission depletion (STED) and structured illumination microscopy (SIM), further improves the spatial resolution of LDs' imaging.[11,18,19] However, they were constrained within shallow imaging depth due to large scattering effect of short wavelength. As a solution, multi-photon microscopy is an effective way to improve penetration depth owing to its long-wavelength excitation and nonlinear confinement. Two-photon microscopy (2PM) to LDs has been successfully used in cells, mouse tissues, and living zebrafish with good performance.[13,15–17] Moreover, three-photon microscopy (3PM) holds an even larger penetration depth than 2PM, maintaining high contrast in turbid tissue including mouse brain[20–24] and liver.[25] However, few three-photon fluorescence imaging of LDs were reported,[25] where the imaging depth as well as resolution could be further improved.

In this study, we employed a luminogen named NAP-CF_3 with enhanced fluorescence in oleic acid (OA) for LDs imaging in fatty liver through confocal and three-photon microscopy. Moreover, three-photon fluorescence imaging of LDs in the fatty liver was conducted and reached the largest depth ever reported,[13,24] which would be significant for fatty liver diagnosis and obesity research. The primary objective of this study was to improve the imaging depth of LDs at the tissue level.

2. Methods

2.1. *Materials*

Chemicals and reagents were purchased from qualified chemical sources. NAP-CF_3 was synthesized according to a previously published literature.[26] OA was bought from Sigma-Aldrich (USA). The mouse (C57BL/6JGpt DIO) was purchased from Gem Pharmatech Company.

2.2. *Characterization of NAP-CF_3*

The synthetic process of NAP-CF_3 was referred to our previous work.[26] The absorption spectra of NAP-CF_3 were recorded by a UV–vis–NIR scanning spectrophotometer (UV-2550, Shimadzu, Japan), while photoluminescence spectra of the NAP-CF_3 were measured by a HITACHI F-2500 fluorescence spectrophotometer with an excitation wavelength of 405 nm. To measure the fluorescence of the NAP-CF_3 mixture in OA, the same concentration of NAP-CF_3 in dimethyl sulfoxide (DMSO) and OA was illuminated by a Xenon lamp at 405 nm.

2.3. *Confocal imaging*

Confocal fluorescence imaging was conducted on a Zeiss LSM 800 laser confocal microscope. HeLa cells were cultured in standard 5%CO_2/air 37°C environments. NAP-CF_3 (50 nM) and Nile Red (100 nM) were both dispersed in Dulbecco's modified eagle medium (DMEM). HeLa cells were further incubated with these compounds. After incubation, the cells were washed three times with phosphate-buffered saline (PBS, pH = 7.4). To obtain co-stain imaging, NAP-CF_3 was excited by 405-nm laser and

we collected the fluorescence in the 400–500 nm range, while Nile Red was excited by 488 nm laser and its fluorescence was collected in 540–700 nm range.

2.4. *Guinea pig tissue preparation*

The high-fat fed and normal guinea pig tissue samples were obtained from the Experimental Animal Center of Guangzhou University of Chinese Medicine (SYXK (Yue) 2018-0085). 30 Male Hartley guinea pigs were obtained from the Guangdong Experimental Animal Center. The living condition of guinea pigs were at constant temperature (20–25°C) and 65–70% humidity with a 12-h light/dark cycle in independent ventilation cage. After one week of adaptive feeding, all guinea pigs were randomly divided into control group (5 guinea pigs) and experimental group (25 guinea pigs). The control group was under normal diet whereas the experimental group was under high-fat diet. The guinea pigs were anesthetized with 10% chloral hydrate (0.3 mL/100 g), and the whole livers were taken every week for five weeks.

The frozen liver tissue was embedded with optical cutting temperature (OCT) agent in a cryostat (Thermo Scientific, USA) and sectioned with the thickness of 10 μm. Tissue samples were stained with the culture medium containing 1 μM of NAP-CF_3 in 5% CO_2/air humidified incubator at 37°C for 1 h. The tissues were washed three times with PBS (pH = 7.4) prior to imaging. Fluorescent images were obtained on Zeiss LSM 800 confocal scanning microscope (excitation = 405 nm and emission collection = 480–560 nm for NAP-CF_3).

2.5. *Three-photon fluorescence characterization of NAP-CF_3*

The glass capillaries contained NAP-CF_3 in DMSO, and OA were imaged under a 3PF microscopy. The 3PF images were recorded under different excitation powers to get the P-I relationship of NAP-CF_3.

The comparison method was applied to measure σ_3 of NAP-CF_3 according to our previous work.[27] Fluorescein in saline solution at 1300 nm was selected as the reference.[28] NAP-CF_3 in DMSO and fluorescein in saline solution were excited by the 1300 nm fs laser, and their 3PF signals were collected by a photomultiplier tube (PMT). The mean 3PF intensities were calculated by ImageJ. The σ_3 value of NAP-CF_3 was calculated by the following equation:

$$\sigma_{3_1} = \sigma_{3_0} \frac{F_1 \eta_0 c_0 n_0}{F_0 \eta_1 c_1 n_1}, \tag{1}$$

where F is the 3PF intensity, η is the fluorescence quantum yield, c is the molar concentration of sample, n is the refractive index of the solvent, and the subscripts 1 and 0 represent NAP-CF_3 and fluorescein, respectively.

σ_3 of NAP-CF_3 at other excitation wavelengths were referenced to the value at 1300 nm measured above and calculated by the following equation:

$$\sigma_{3,\lambda} = \sigma_{3,1300} \frac{P_{1300}^3 \tau_\lambda^2 F_\lambda}{P_\lambda^3 \tau_{1300}^2 F_{1300}} \left(\frac{\lambda}{1300}\right)^3, \tag{2}$$

where $\sigma_{3,\lambda}$ is the wavelength dependent three-photon absorption cross-section, $\sigma_{3,1300}$ is σ_3 of NAP-CF_3 at 1300 nm, P_{1300} and P_λ are the time-averaged excitation photon flux (photons/s) on the sample, τ_{1300} and τ_λ are the measured pulse widths on the sample, and F_{1300} and F_λ are the measured 3PF intensities with excitation at 1300 nm and other wavelengths, respectively.

The 3PF photostability of NAP-CF_3 was tested as following. 0.1 mg/mL NAP-CF_3 in OA was contained in a tube capillary and imaged for 24 min continuously under the 1300-nn-fs excitation (average power: 10 mW). The fluorescence intensity was taken from the average intensity of the pixel counts on tube capillary in the field of view (Zoom = 1). Dwell time = 2.2 μs/pixel; field of view: 480 × 480 μm; frame rate: 4 frame/slice.

2.6. *Three-photon fluorescence imaging of mice liver tissue*

The adult model mouse (C57BL/6JGpt DIO) was sacrificed to obtain the fresh mice liver tissues. Immediately, the tissues were incubated with NAP-CF_3 (100 nM) at room temperature in culture medium (DMEM) for 2 h. Afterwards, the tissues were washed with PBS (pH = 7.4) before three-photon fluorescence imaging. The 3PM used a non-collinear optical parametric amplifier (NOPA) with wavelength-tunable femtosecond (fs) laser output and a commercial Bruker scanning microscope. The

NOPA part consisted of a 1030-nm fs pump laser (Spectra-Physics, Spirit) and an optical parametric amplifier system (Spectra-Physics, NOPA-VISIR). 1300-nm fs laser beam was selected as the excitation source and a 60X oil objective (Filling factor = 1; effective NA = 1.35, UPlanSApo60X, Olympus) was applied for high-magnified fluorescence imaging. The full width at half maximum of 1300-nm fs laser beam was measured as 115 fs after the objective. Laser power before objective: 15 mW for 0–30 μm imaging, 30 mW for 31–45 μm imaging, 60 mW for 46–60 μm imaging, and 90 mW for 61–80 μm imaging. The experiments above were performed in compliance with the ethical standards of the Institutional Ethical Committee of Animal Experimentation of Zhejiang University (ZJU-IACUC: ZJU20210222).

3. Results and Discussions

The structure of NAP-CF_3 is shown in Fig. 1(a). The normalized extinction and FL spectra of NAP-CF_3 have been demonstrated in our previous work.[26] We first testified the fluorescent enhancement of NAP-CF_3 when bound to LDs. Figure 1(a) showed the extinction spectra of NAP-CF_3 in DMSO and OA. NAP-CF_3 showed an absorption peak at around 420 nm both in DMSO and OA. There is little difference in the extinction spectral shape. However, the fluorescence of NAP-CF_3 in OA showed a strongly enhanced intensity compared with that of NAP-CF_3 in DMSO [Fig. 1(b)]. The blue-shifted and enhanced fluorescence of NAP-CF_3 in OA is attributed to the nonpolar character of OA and solvatochromic property of NAP-CF_3.

With enhanced emission in OA, NAP-CF_3 could possibly target to LDs specifically, since the viscosity inside LD is very high. Our previous work have confirmed a high clog P value of NAP-CF_3.[26] Therefore, NAP-CF_3-labeled LDs possibly have extremely high contrast in imaging.[26] To illustrate it, we performed the co-staining LD imaging with commercially available LD-labeled probe, Nile Red (Fig. 2). As shown in Figs. 2(a) and 2(b), LDs were clearly stained with NAP-CF_3 and Nile Red. The merged imaging in Fig. 2(c) demonstrated that the fluorescence of NAP-CF_3 and Nile Red were overlapped well, confirming the high staining specificity of NAP-CF_3 to LDs. The enlarged images in Figs. 2(d)–2(f) showed LDs with high spatial resolution. In Fig. 2(d), other parts which were out of LDs emitted little fluorescence. As shown in Fig. 2(h), NAP-CF_3 displayed clear background, whereas Nile-Red showed partly nonspecific fluorescence from cells that are stained with LDs. The case above verified the enhanced fluorescence of NAP-CF_3 when binding to LDs.

Sequentially, we monitored the development process of fatty liver through confocal microscopy. As shown in Fig. 3, small LDs could be discriminated at an early stage (Week 1). Over time, the size and density of LDs grew bigger and higher. Finally, the fatty liver was full of large LDs, indicating that the fatty liver was mature. High-

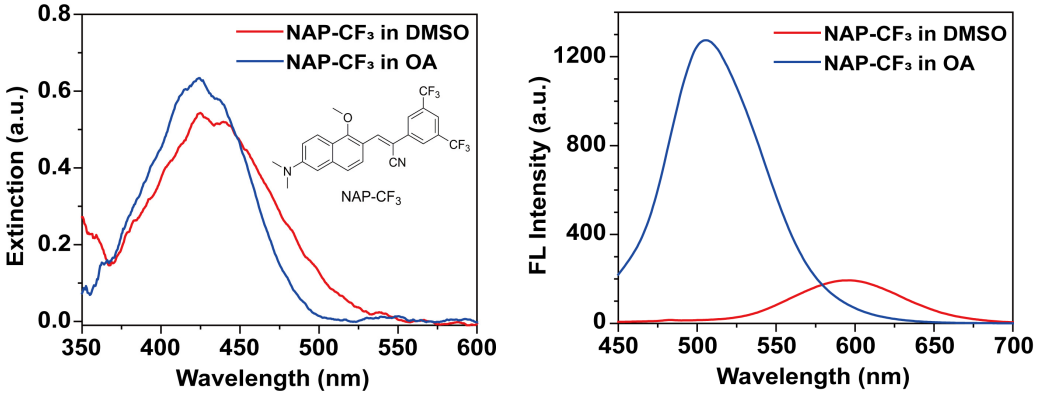

(a) (b)

Fig. 1. Optical characterization of NAP-CF_3. (a) The extinction spectra of NAP-CF_3 in DMSO and oleic acid (OA). The concentration of NAP-CF_3 is 10 μg/mL, optical length = 1 mm. Insert: The structure of NAP-CF_3. (b) The fluorescence spectra of NAP-CF_3 (10 μg/mL) in DMSO and OA (Excitation wavelength is 420 nm).

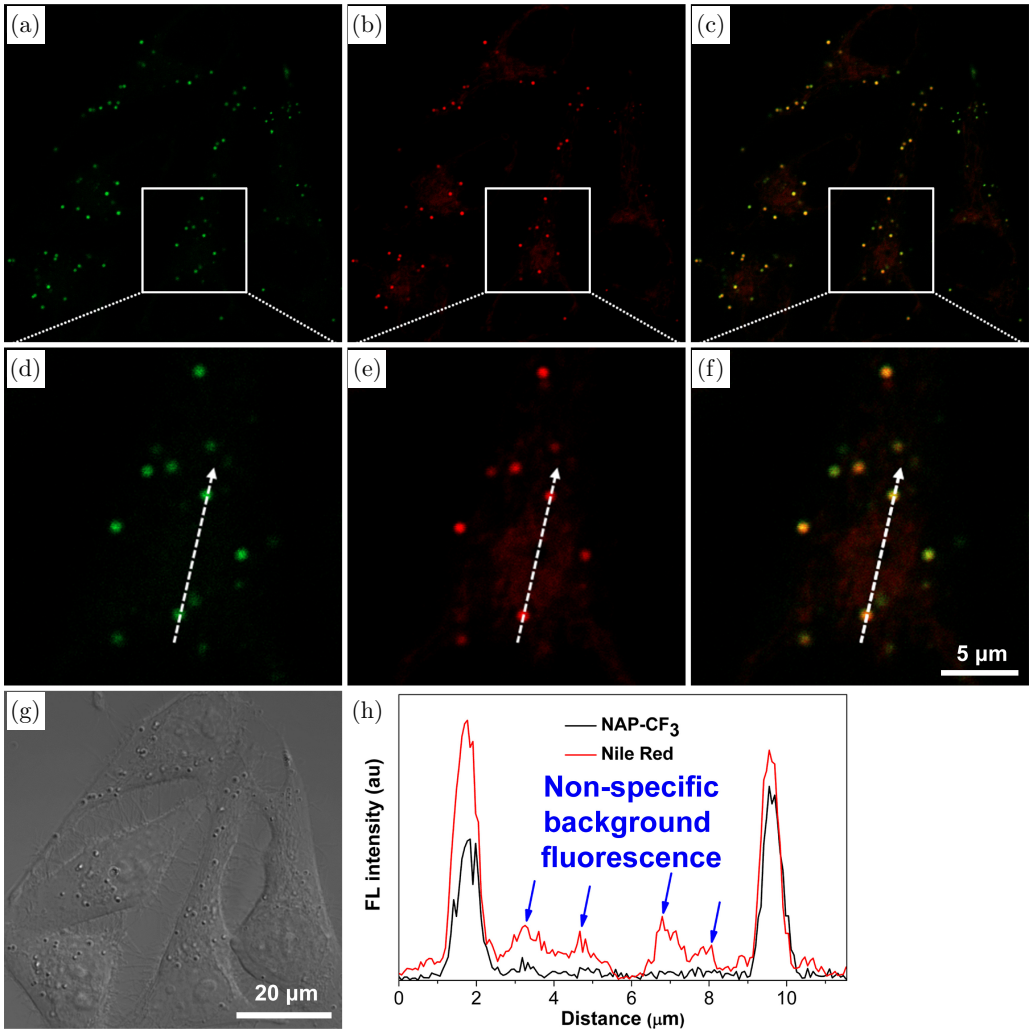

Fig. 2. Colocalized and zoomed-in confocal laser scanning microscope images ($\lambda_{ex} = 405$ nm for NAP-CF_3 and $\lambda_{ex} = 488$ nm for Nile-Red) of HeLa cells stained with (a, d) NAP-CF_3 (50 nM) and (b, e) Nile Red (100 nM). (c, f) merged images obtained from two different fluorescent panels and (g) image obtained from the bright field. (h) Fluorescent intensity obtained from NAP-CF_3 and Nile-Red.

contrast LDs imaging labeled by NAP-CF_3 successfully monitored the fatty liver at different stages, ensuring the high efficiency of fatty liver diagnosis.

Although confocal imaging of LDs could realize fatty liver diagnosis, the imaging was constricted within shallow slices (within 10-μm thickness). However, multi-photon imaging allows imaging with larger depth. Therefore, we tested multi-photon absorption performance of NAP-CF_3. First, we measured the power dependence relationship between the fluorescence intensity of NAP-CF_3 and the excitation intensity. The fitted curve between logarithm of the fluorescence intensity and the excitation intensity was measured with a slope of 2.91 in Fig. 4(a), which indicated that a major three-photon absorption process happened under 1300-nm fs excitation. We then measured three-photon absorption cross-section (σ_3) spectrum of NAP-CF_3 through comparison method reported previously.[27] The results showed that NAP-CF_3 had peak σ_3 at 1300 nm. The σ_3 at 1300 nm was calculated to be 1.67×10^{-79} $cm^6 s^2$, which is larger than most of commercial fluorophores.[22] Moreover, we compared three-photon fluorescence imaging of NAP-CF_3 in DMSO and OA. The three-photon fluorescence of NAP-CF_3 in OA was brighter than it in DMSO. Fluorescence intensity of NAP-CF_3 in OA in Fig. 4(c) was 2.2 times as high as the fluorescence intensity of NAP-CF_3 in DMSO. The NAP-CF_3 in OA also showed excellent photostability under

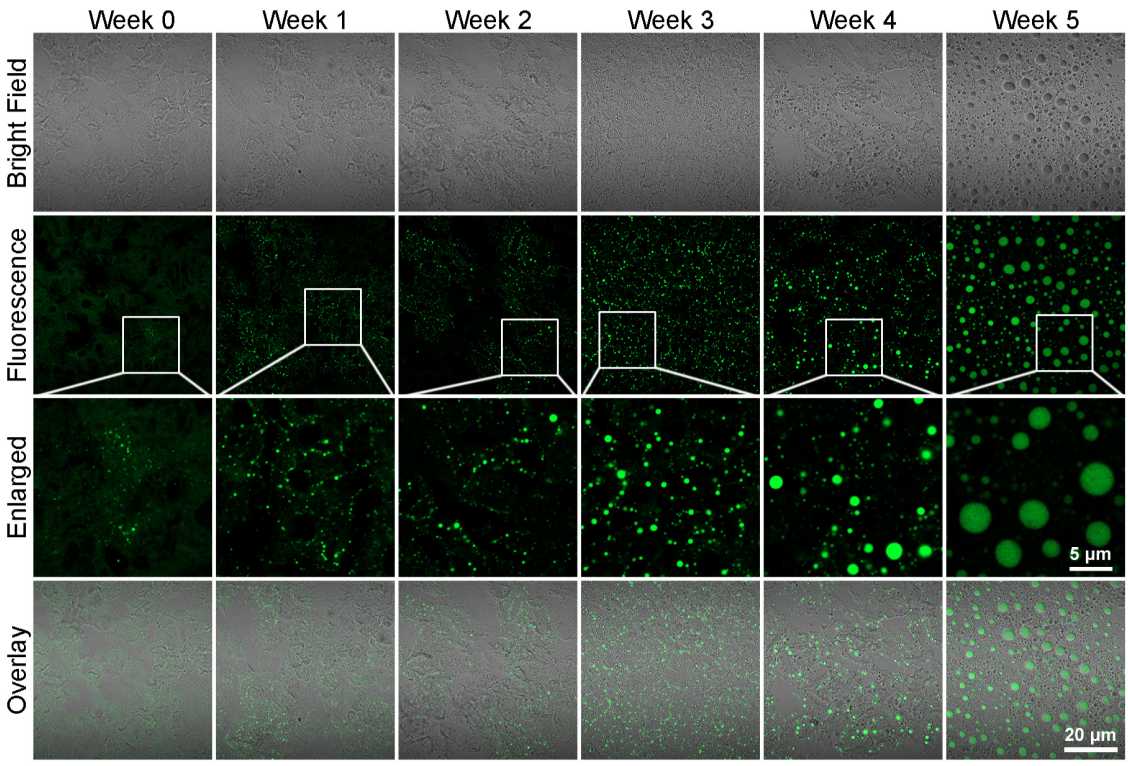

Fig. 3. Confocal laser scanning microscopic images ($\lambda_{ex} = 405$ nm) of high-fat feeding control (Week 0) and experimental (Week 1 to Week 5) guinea pig liver tissues stained with NAP-CF_3 (50 nM) within 10-μm depth.

continuous 1300 nm fs excitation for more than 20 min in Fig. 4(d), where a power intensity of 10 mW is enough for three-photon imaging of LDs in liver tissues. The three-photon fluorescence had only been bleached by less than 15%. The remarkable three-photon performance of NAP-CF_3 guarantees its potential for 3PF LDs imaging.

Given its remarkable 3PF imaging performance, we further performed three-photon fluorescence imaging of LDs in liver tissues. The intensity of 3PF mainly constrains the imaging depth, while the emission wavelength plays a small role because the emission wavelength from green to red in 3PM does not significantly influence the fluorescence collection

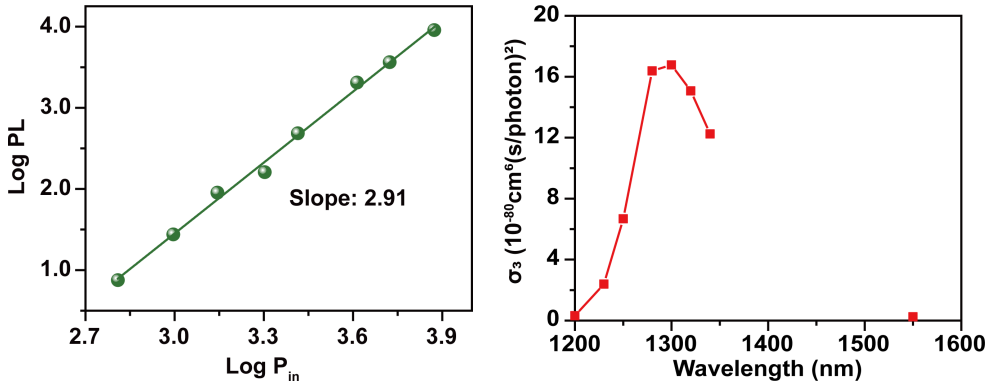

(a) (b)

Fig. 4. (a) The logarithm of the fluorescence intensity of NAP-CF_3 against that of the 1300-nm fs excitation intensity curve. (b) The three-photon absorption cross-section spectrum of NAP-CF_3 in DMSO. (c) Quantitative analysis of fluorescence intensity of NAP-CF_3 (10 μg/mL) in DMSO and OA. Insert: three-photon fluorescence imaging of NAP-CF_3 (10 μg/mL) in DMSO and OA under 1300-nm fs excitation. (d) Photostability of NAP-CF_3 (10 μg/mL) in OA under the continuous irradiation of 1300 nm fs laser (Average power: 10 mW).

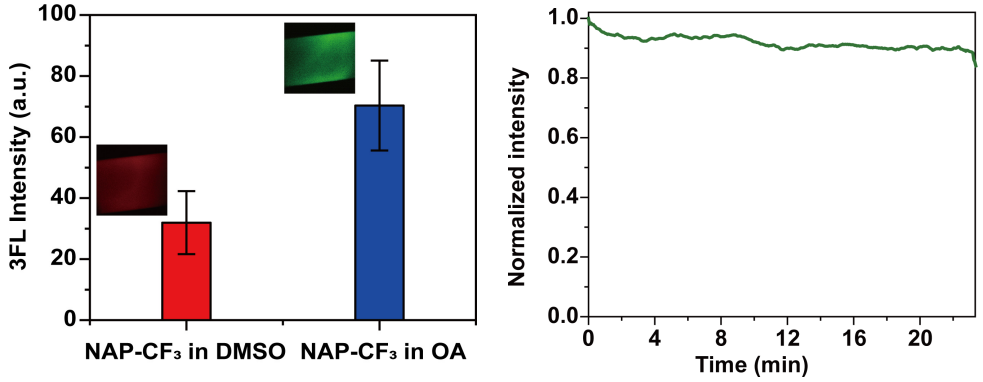

(c) (d)

Fig. 4. (*Continued*)

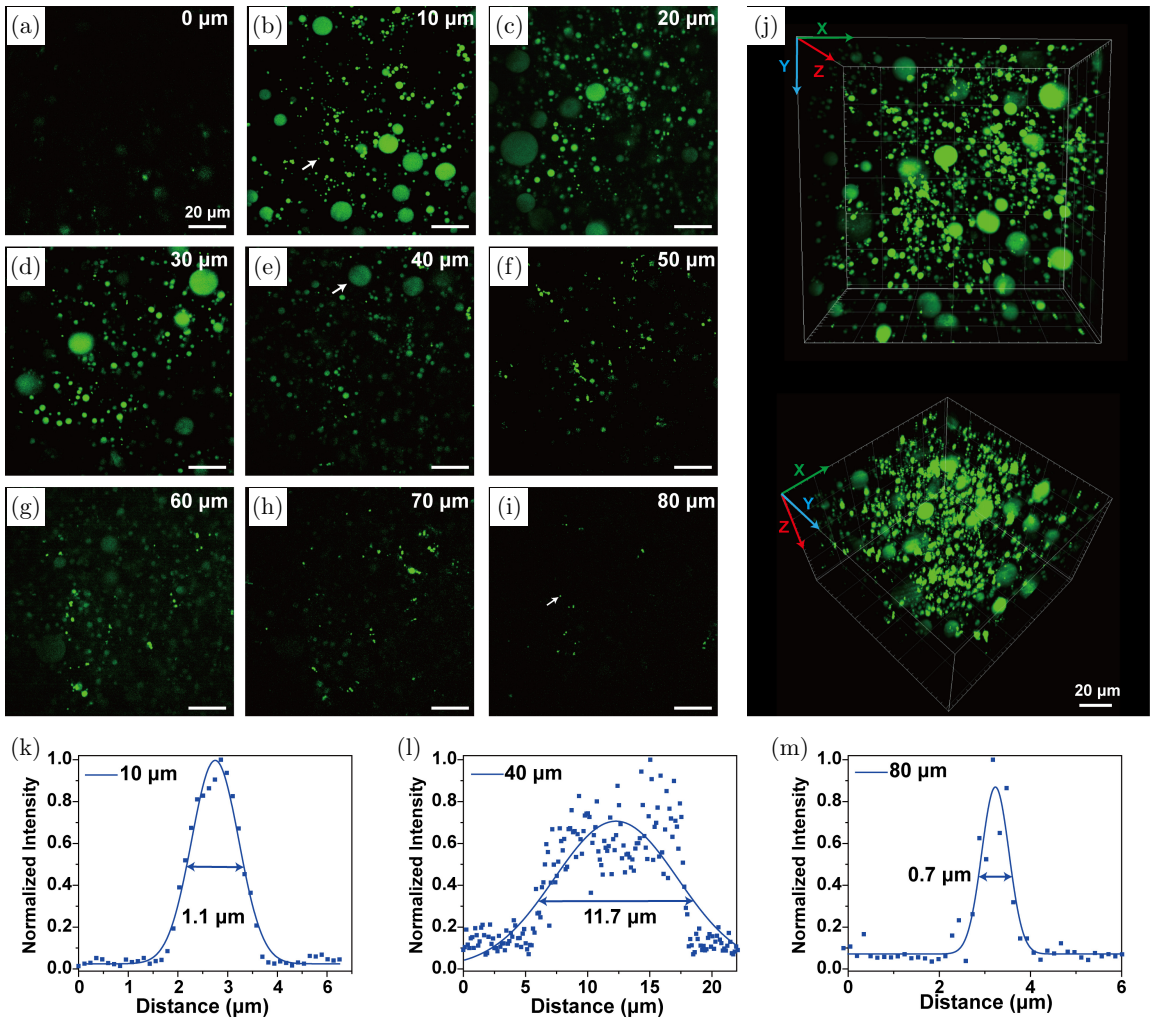

Fig. 5. *Ex vivo* three-photon fluorescence imaging of LDs in live mice fatty liver tissues. (a–i) Three-photon fluorescence microscopic imaging of LDs from 0 to 80 μm depth. (j) Reconstructed 3D three-photon fluorescence imaging of LDs (0–80 μm). (k–m) Gaussian analysis of arrow-pointed LD at imaging depth of 10 μm (b), 40 μm (e), and 80 μm (i).

efficiency.[29] Thus, the blue shift of NAP-CF_3 in OA would not hinder the 3PF imaging depth. Due to the enhanced three-photon fluorescence intensity of NAP-CF_3 in OA, deep LDs imaging was carried out in Fig. 5. The high nonlinear effect of 3PM guarantees good optical tomographic capability. Three-photon fluorescence imaging of LDs at different depths from 0 to 80 μm was shown with high contrast in Figs. 5(a)–5(i). Single LD as small as 1.1 μm was shown with high SBR [Fig. 5(k)]. Big LD at depth of 40 μm was also analyzed and was measured to be 11.7 μm [Fig. 5(l)]. Even small LD at depth of 80 μm was distinguishable with large SBR around 12 [Fig. 5(m)]. Finally, the reconstructed 3D images of LDs in Fig. 5(j) clearly showed the distribution of LDs. The effective attenuation length of 3PF imaging in liver was measured as around 15.0 μm, which demonstrated very high turbidity of liver tissue. *In vivo*, three-photon fluorescence imaging of LDs in our work was not achieved due to the fast jitter caused by mouse's breathing. Three-photon fluorescence imaging of LDs demonstrated lots of advantages, including high contrast, high resolution, and large imaging depth.

4. Conclusion

Our study demonstrated excellent imaging performances of NAP-CF_3 in precise high-resolution confocal imaging *in vitro*, and three-photon fluorescence imaging of LDs *ex vivo*. Due to the high specificity of this marker for LDs staining, the background fluorescence interference in imaging is dramatically reduced compared with commercial Nile Red. Meanwhile, the high specificity of NAP-CF_3 to LDs guarantees the diagnosis of fatty liver at an early stage. Three-photon fluorescence imaging promotes LDs imaging to a large depth. The high resolution and deep-tissue imaging of LDs achieved using NAP-CF_3 are important for future LDs-assisted pathologies research.

Conflicts of Interest

There are no conflicts to declare.

Acknowledgments

This work was supported by National Natural Science Foundation of China (61975172, 82001874, 62105184), and the Guangdong Basic and Applied Basic Research Foundation (2020A1515110578). We thank Prof. Shijie Li from Guangzhou University of Chinese Medicine for giving helpful advices to perform the tissue imaging experiments. M. He and H. Park contributed equally to this paper.

References

1. A. R. Thiam, R. V. Jr. Farese, T. C. Walther, "The biophysics and cell biology of lipid droplets," *Nat. Rev. Mol. Cell Biol.* **14**(12), 775–786 (2013).
2. R. V. Jr. Farese, T. C. Walther, "Lipid droplets finally get a little R-E-S-P-E-C-T," *Cell* **139**(5), 855–860 (2009).
3. T. C. Walther, R. V. Jr. Farese, "Lipid droplets and cellular lipid metabolism," *Annu. Rev. Biochem.* **81**, 687–714 (2012).
4. J. A. Olzmann, C. M. Richter, R. R. Kopito, "Spatial regulation of UBXD8 and p97/VCP controls ATGL-mediated lipid droplet turnover," *Proc. Natl. Acad. Sci. USA* **110**(4), 1345–1350 (2013).
5. N. Krahmer, R. V. Jr. Farese, T. C. Walther, "Balancing the fat: Lipid droplets and human disease," *EMBO Mol. Med.* **5**(7), 973–983 (2013).
6. S. Daemen, M. van Zandvoort, S. H. Parekh, M. K. C. Hesselink, "Microscopy tools for the investigation of intracellular lipid storage and dynamics," *Mol. Metab.* **5**(3), 153–163 (2016).
7. W. Li, B. J. Dobraszczyk, P. J. Wilde, "Surface properties and locations of gluten proteins and lipids revealed using confocal scanning laser microscopy in bread dough," *J. Cereal Sci.* **39**(3), 403–411 (2004).
8. P. Raudsepp, D. A. Brüggemann, M. L. Andersen, "Detection of radicals in single droplets of oil-in-water emulsions with the lipophilic fluorescent probe BODIPY665/676 and confocal laser scanning microscopy," *Free Radic. Biol. Med.* **70**, 233–240 (2014).
9. E. Kim, S. Lee, S. B. Park, "A Seoul-Fluor-based bioprobe for lipid droplets and its application in image-based high throughput screening," *Chem. Commun.* **48**(17), 2331–2333 (2012).
10. C. Zhang, J. Li, L. Lan, J. X. Cheng, "Quantification of lipid metabolism in living cells through the dynamics of lipid droplets measured by stimulated raman scattering imaging," *Anal. Chem.* **89**(8), 4502–4507 (2017).
11. Y. Xu, H. Zhang, N. Zhang, R. Xu, Z. Wang, Y. Zhou, Q. Shen, D. Dang, L. Meng, B. Z. Tang, "An easily synthesized AIE luminogen for lipid droplet-specific super-resolution imaging and two-photon

imaging, *Mater. Chem. Front.* **5**(4), 1872–1883 (2021).
12. S. Zhang, Z. Yang, M. Li, Q. Zhang, X. Tian, D. Li, S. Li, J. Wu, Y. Tian, "A multi-photon fluorescent probe based on quinoline groups for the highly selective and sensitive detection of lipid droplets," *Analyst* **145**(24), 7941–7945 (2021).
13. Y. Yu, H. Xing, H. Park, R. Zhang, C. Peng, H. H. Y. Sung, I. D. Williams, C. Ma, K. S. Wong, S. Li, Q. Xiong, M.-H. Li, Z. Zhao, B. Z. Tang, "Deep-red aggregation-induced emission luminogen based on dithiofuvalene-fused benzothiadiazole for lipid droplet-specific imaging," *ACS Mater. Lett.* **4**(1), 159–164 (2022).
14. M. Jiang, X. Gu, J. W. Y. Lam, Y. Zhang, R. T. K. Kwok, K. S. Wong, B. Z. Tang, "Two-photon AIE bio-probe with large Stokes shift for specific imaging of lipid droplets," *Chem. Sci.* **8**(8), 5440–5446 (2017).
15. H. Park, S. Li, G. Niu, H. Zhang, Z. Song, Q. Lu, J. Zhang, C. Ma, R. T. K. Kwok, J. M. Y. Lam, K. S. Wong, X. Yu, Q. Xiong, B. Z. Tang, "Diagnosis of fatty liver disease by a multiphoton-active and lipid-droplet-specific AIEgen with nonaromatic rotors," *Mater. Chem. Front.* **5**(4), 1853–1862 (2021).
16. T. Shao, T. Liu, H. Liu, M. Zhang, Y. Shen, A. Gao, X. Tian, Q. Zhang, J. Wu, Y. Tian, "Identification of fatty liver disease at diverse stages using two-photon absorption of triphenylamine-based BODIPY analogues," *J. Mater. Chem. B* **7**(23), 3704–3709 (2019).
17. L. Guo, M. Tian, R. Feng, G. Zhang, R. Zhang, X. Li, Z. Liu, X. He, J. Z. Sun, X. Yu, "Interface-targeting strategy enables two-photon fluorescent lipid droplet probes for high-fidelity imaging of turbid tissues and detecting fatty liver," *ACS Appl. Mater. Interfaces* **10**(13), 10706–10717 (2018).
18. M.-Y. Wu, J.-K. Leung, C. Kam, T. Y. Chou, D. Wang, S. Feng, S. Chen, "A near-infrared AIE probe for super-resolution imaging and nuclear lipid droplet dynamic study," *Mater. Chem. Front.* **5**(7), 3043–3049 (2021).
19. X. Nan, E. O. Potma, X. S. Xie, "Nonperturbative chemical imaging of organelle transport in living cells with coherent anti-stokes raman scattering microscopy," *Biophys. J.* **91**(2), 728–735 (2006).
20. M. Liu, B. Gu, W. Wu, Y. Duan, H. Liu, X. Deng, M. Fan, X. Wang, X. Wei, K.-T. Yong, K. Wang, G. Xu, B. Liu, "Binary organic nanoparticles with bright aggregation-induced emission for three-photon brain vascular imaging," *Chem. Mater.* **32**(15), 6437–6443 (2020).
21. L. Streich, J. C. Boffi, L. Wang, K. Alhalaseh, M. Barbieri, R. Rehm, S. Deivasigamani, C. T. Gross, A. Agarwal, R. Prevedel, "High-resolution structural and functional deep brain imaging using adaptive optics three-photon microscopy," *Nat. Methods* **18**(10), 1253 (2021).
22. Y. Hontani, F. Xia, C. Xu, "Multicolor three-photon fluorescence imaging with single-wavelength excitation deep in mouse brain," *Sci. Adv.* **7**(12), eabf3531 (2021).
23. Z. L. Qiu, M. B. He, K. S. Chu, C. Tang, X. W. Chen, L. Zhu, L. P. Zhang, D. Sun, J. Qian, Y. Z. Tan, "Well-defined segment of carbon nanotube with bright red emission for three-photon fluorescence cerebrovascular imaging," *Adv. Opt. Mater.* **9**(19), 2100482 (2021).
24. N. G. Horton, K. Wang, D. Kobat, C. G. Clark, F. W. Wise, C. B. Schaffer, C. Xu, "In vivo three-photon microscopy of subcortical structures within an intact mouse brain," *Nat. Photonics* **7**(3), 205–209 (2013).
25. S. Wang, X. Li, S. Y. Chong, X. Wang, H. Chen, C. Chen, L. G. Ng, J. W. Wang, B. Liu, "In vivo three-photon imaging of lipids using ultrabright fluorogens with aggregation-induced emission," *Adv. Mater.* **33**(11), e2007490 (2021).
26. G. Niu, R. Zhang, J. P. C. Kwong, J. W. Y. Lam, C. Chen, J. Wang, Y. Chen, X. Feng, R. T. K. Kwok, H. H. Y. Sung, I. D. Williams, M. R. J. Elsegood, J. Qu, C. Ma, K. S. Wong, X. Yu, B. Z. Tang, "Specific two-photon imaging of live cellular and deep-tissue lipid droplets by lipophilic AIEgens at ultralow concentration," *Chem. Mater.* **30**(14), 4778–4787 (2018).
27. M. He, D. Li, Z. Zheng, H. Zhang, T. Wu, W. Geng, Z. Hu, Z. Feng, S. Peng, L. Zhu, W. Xi, D. Zhu, B. Z. Tang, J. Qian, "Aggregation-induced emission nanoprobe assisted ultra-deep through-skull three-photon mouse brain imaging," *Nano Today* **45**, 101536 (2022).
28. L.-C. Cheng, N. G. Horton, K. Wang, S.-J. Chen, C. Xu, "Measurements of multiphoton action cross sections for multiphoton microscopy," *Biomed. Opt. Express* **5**(10), 3427–3433 (2014).
29. M. Wang, M. Kim, F. Xia, C. Xu, "Impact of the emission wavelengths on in vivo multiphoton imaging of mouse brains," *Biomed. Opt. Express* **10**(4), 1905–1918 (2019).